WISDOM: the WIYN Spectrograph for DOppler Monitoring – a NASA-NSF concept for an extreme precision radial velocity instrument in support of TESS

Gábor Fűrész [a], Robert Simcoe [a], Stuart I. Barnes [b], Lars A. Buchhave [c], Mark Egan [a], Rick Foster [a], Tim Hellickson [a], Andrew Malonis [a], David Phillips [d], Steve Shectman [e], Ronald Walsworth [d], Josh Winn [a], and Deborah F. Woods [f]

[a] MIT Kavli Institute for Astrophysics and Space Research, 77 Mass. Ave, Cambridge, MA 02139, United States;
[b] Stuart Barnes optical Design (Germany);
[c] University of Copenhagen (Denmark);
[d] Harvard-Smithsonian Center for Astrophysics (United States);
[e] Carnegie Observatories (United States);
[f] MIT Lincoln Laboratory (United States).
contact: gfuresz@mit.edu

ABSTRACT

The Kepler mission highlighted that precision radial velocity (PRV) follow-up is a real bottleneck in supporting transiting exoplanet surveys. The limited availability of PRV instruments, and the desire to break the "1 m/s" precision barrier, prompted the formation of a NASA-NSF collaboration 'NN-EXPLORE' to call for proposals designing a new Extreme Precision Doppler Spectrograph (EPDS). By securing a significant fraction of telescope time on the 3.5m WIYN at Kitt Peak, and aiming for unprecedented long-term precision, the EPDS instrument will provide a unique tool for U.S. astronomers in characterizing exoplanet candidates identified by TESS. One of the two funded instrument concept studies is led by the Massachusetts Institute of Technology, in consortium with Lincoln Laboratories, Harvard-Smithsonian Center for Astrophysics and the Carnegie Observatories. This paper describes the instrument concept WISDOM (WIYN Spectrograph for DOppler Monitoring) prepared by this team.

WISDOM is a fiber fed, environmentally controlled, high resolution (R=110k), asymmetric white-pupil echelle spectrograph, covering a wide 380-1300nm wavelength region. Its R4 and R6 echelle gratings provide the main dispersion, symmetrically mounted on either side of a vertically aligned, vacuum-enclosed carbon fiber optical bench. Each grating feeds two cameras and thus the resulting wavelength range per camera is narrow enough that the VPHG cross-dispersers and employed anti-reflection coatings are highly efficient. The instrument operates near room temperature, and so thermal background for the near-infrared arm is mitigated by thermal blocking filters and a short (1.7μm) cutoff HgCdTe detector. To achieve high resolution while maintaining small overall instrument size (100/125mm beam diameter), imposed by the limited available space within the observatory building, we chose to slice the telescope pupil 6 ways before coupling light into fibers. An atmospheric dispersion corrector and fast tip-tilt system assures maximal light gathering within the 1.2″ entrance aperture. The six octagonal fibers corresponding to each slice of the pupil employ ball-lens double scramblers to stabilize the near- and far-fields. Three apiece are coupled into each of two rectangular fibers, to mitigate modal nose and present a rectilinear illumination pattern at the spectrograph's slit plane. Wavelength solutions are derived from ThAr lamps and an extremely wide coverage dual-channel laser frequency comb. Data is reduced on the fly for evaluation by a custom pipeline, while daily archives and extended scope data reduction products are stored on NExScI servers, also managing archives and access privileges for GTO and GO programs.

Note: individual papers, submitted along this main paper, describe the details of subsystems such as the optical design (Barnes et al., 9908-247), the fiber link design (Fűrész et al., 9908-281), and the pupil slicer (Egan et al., 9912-183).

Keywords: precision radial velocity spectrograph, white pupil echelle spectrograph, high resolution spectroscopy, pupil slicer, fiber fed, near-infrared echelle, EPDS, TESS

1. INTRODUCTION

1.1 EPDS Proposal Requirements

The Kepler mission highlighted that precision radial velocity (PRV) follow-up is a real bottleneck in supporting transiting exoplanet surveys. The limited availability of PRV instruments, and the current ~1m/s observational precision barrier, prompted the formation of a NASA-NSF collaboration 'NN-EXPLORE' to call for proposals designing a new Extreme

Precision Doppler Spectrograph (EPDS) that aims to reach 0.5m/s precision as a requirement with a 0.1m/s goal (hence called "extreme" PRV), excluding astrophysical noise. Such instrument development has been strongly suggested by the 2010 "New Wrolds, New Horizons" Decadal Survey report, as well as the NASA Exoplanet Exploration Program Analysis Group (ExoPAG) white paper[1].

The Announcement of Opportunity (AO) appeared in January, 2015, and called for a 2-step proposal process with a 3-month pre-proposal stage followed by a quick down-select and a 6-month-long, funded ($250k) Instrument Conceptual Study (ICS) phase starting in August, 2015. The final decision on the instrument design and build was scheduled for March, 2016. Just as the proposal process itself, the AO called for a very aggressive instrument design and delivery schedule (<2.5 years) with on-sky commissioning in late 2018/early 2019, mostly driven by the TESS schedule. The AO outlined a tentative $7M budget cap, with the notion not to exclude proposals with a budget bottom line above the proposed limit. (In fact both proposals selected for the funded ICS phase were significantly above that limit, while being very consistent with each other).

By securing a significant fraction of telescope time on the 3.5m WIYN at Kitt Peak over the 7-year NN-EXPLORE program, the EPDS instrument was meant to provide a unique tool for U.S. astronomers in characterizing exoplanet candidates identified by TESS and also to support JWST observations. The choice of the WIYN telescope imposed some requirements on the design, like: the lack of good telescope throughput below 380nm wavelength; use of a folded Cassegrain port with specific weight and moment for the front end (<400kg, <2000Nm); a relatively small and odd-shaped spectrograph room (~12m^2) with a minimum of 27m fiber length; and a median seeing condition of 0.7″ with a specific PSF profile; etc.

Besides the aforementioned RV precision requirement/goal, budget guideline, interface constraints, a minimum spectral resolution value of R>70k and use of a fiber feed the definition of instrument parameters were left to the proposing teams, as well as the development of a science case. Thus our approach was to define a sound scientific program, and then derive the instrument parameters from our own science goals and deduced observing requirements.

1.2 WISDOM Science Requirements

One of the most surprising and important findings in exoplanetary science is that nearly half of Sun-like stars have at least one planet with an orbital period shorter than one year, and a size in between that of Earth and Neptune[2]. Little is known about this new category of planets, as there is no local example in the Solar System. Their orbital parameters are poorly measured, and their constitutions and atmospheres are mysterious.

Starting in 2018, TESS will identify hundreds of small planets around nearby, bright stars. The task of measuring planet masses will be severely limited by the available telescope time and achievable radial velocity precision. For the smallest planetary signals (<1 m/s) we will also be limited by our ability to identify and correct for the effects of "stellar jitter," the spurious Doppler shifts produced by stellar granulation, magnetic activity, and other astrophysical variations. It is important to overcome this limitation quickly, not only out of the desire for rapid scientific progress, but also to establish the best and brightest targets for the JWST mission (2018-2023). The JWST offers outstanding prospects for transit/occultation spectroscopy of small planets —and for searching the atmospheres of habitable-zone planets for biomarkers— but only if the brightest and most favorable systems are detected and confirmed in time.

Further ahead, the WFIRST-AFTA coronagraph will be capable of imaging and spectroscopy of wide-orbiting giant planets, including exoplanetary analogs of Jupiter and Saturn[3]. However, most of the candidate target stars have not yet been included in Doppler surveys, and consequently little is known about the relevant population of planets. A long-term Doppler survey of potential WFIRST-AFTA targets would be a vital contribution to the mission, by allowing the space telescope to concentrate on planet characterization rather than discovery. Since the relevant orbital periods are 5-20 years, the Doppler program must begin soon, even though the WFIRST-AFTA mission will likely not begin until the mid-2020s.

Table 1 summarizes the expected characteristics of the most important types of stars and planets for these missions. Based on such expectations, the most important characteristics for a precise Doppler spectrograph are:

Time Frame	Mission	Types of Stars	Desired PRV Support
2018-2020	TESS	FGK dwarfs (I = 6-13) M dwarfs (K = 5-11)	Detect ≈ 50 signals with K ~ 1 m/s, P = 0.5-20 days
2018-2023	JWST	Brightest M dwarfs with small transiting planets, particularly in the habitable zone (K ≈ 6)	Conclusive stellar and planetary characterization of the most interesting and favorable transiting-planet systems, e.g., a super-Earth in the HZ of an M0 star (K ~ 1m/s, P ~ 60days)
2025-2030	WFIRST-AFTA Coronagraph	Dwarf and subgiants of all spectral types (V = 0-6)	Long term monitoring of 100 targets over several years with ~ 1 m/s precision

Table 1. Summary of target characteristics and required support for current and planned NASA exoplanet missions.

1) Capability to **measure radial velocity (RV) with a precision of 0.5 m/s** or better, to enable the detection of TESS planets comparable in mass to the Earth in short periods, and long-term trends of distant giant planets.
2) Capability for efficient **observations of stars over a wide range of apparent magnitudes**, from V = 0-6 to 6-13. For bright stars, overheads must be short and it must be possible to integrate long enough to average over *p*-mode oscillations. For faint stars, the throughput must be as high as possible.
3) **High spectral resolution and sampling**, allowing for:
   a) Optimal extraction of RV information for a wide variety of stars, including ones with intrinsically narrow absorption lines and slow rotation.
   b) Accurate determination of stellar properties, because the uncertainties in the stellar parameters directly affect the accuracy of the derived planetary parameters.
   c) Transmission spectroscopy of planetary atmospheres, which are expected to have intrinsically narrow features due to low pressure broadening.
   d) Detailed studies of stellar absorption line profiles (such as bisector analyses), to enable the recognition and possible correction of stellar jitter.
4) **Broad wavelength coverage**, including near-infrared (NIR) wavelengths, for multiple reasons:
   a) Enhancing throughput and increasing RV precision by making use of greater portion of the stellar spectrum.
   b) Recognizing and reducing the impact of spurious RV variation due to photospheric/chromospheric variations, which generally weaken with wavelength ($\sim 1/\lambda$).
   c) Facilitating observations of M dwarfs (which are brighter at red and infrared wavelengths), the type of star for which habitable-zone planets are most readily studied.
   d) Facilitating more accurate spectral characterization (mass, radius, surface gravity, and abundances) of planet-hosting stars, as relatively poor characterization of planet-hosting stars is a key limiting factor in the interpretation of transit surveys.

Somewhat alarmingly no Guaranteed Time Observing (GTO) of this non-PI instrument was specified as part of the announcement of opportunity, and discussions about the amount of nights allocated to the instrument team was postponed to be part of the final, build-contract negotiation, only allowing a simple suggestion for GTO time as part of the proposal. Therefore we estimated how much observing time is needed to measure the masses of the potentially habitable TESS planets (as the primary objective), and the most favorable planets spanning a range of sizes from Earth to Neptune (as the secondary objective). For this we used analytical methods and comparison of similar estimates to actual observing data listed in the literature for all Doppler mass measurements of transiting planets smaller than 3 R_E. Evidently, observers have found it necessary to obtain approximately twice as much data as predicted by idealized S/N ratio calculations, which is likely due to stellar activity. According to our simulations[4] there is a subset of ~60 *TESS* planets spanning the 1–4 R_E size range for which masses can be measured at the 20% level with an investment of ~20 hours of observing time each. Therefore, we proposed a 40 night/year GTO program for 5 years, resulting characterization of 40% of the total number of planets needed to satisfy the NASA's Level 1 Requirement for TESS.

1.3 Requirements Flow-down: the Instrument Definition Process

From the AO-defined high level Program Requirements and our own Science Requirements we have flown down instrument specific requirements that outlined the subsystems and defined specific design parameters:

Spectral Resolution (R=110,000 baseline, 160,000 High Resolution): In theory, an *R*=100,000 spectrum would resolve absorption features for most slowly rotating stars[5], however, M-K dwarfs can exhibit even narrower lines[6] motivating a higher resolution capability. A High Resolution (HR) mode is achieved by inserting a narrow slit at the spectrograph's entrance, decreasing the throughput by 33% but boosting resolution to capture the finest possible RV detail.

Pixel Sampling (3.5 pixels baseline, 2.3 pixels High Resolution): Practical experience with PRV instruments suggests that Nyquist-sampled observations rarely achieve their theoretical velocity precision. This is probably because of marginally-sampled line profile variations arising from contrasting features on the stellar photosphere (e.g., starspots), convolved with the velocity profile of stellar rotation and activity.

Wide Passband (380-1300 nm): Most Doppler spectrographs operate almost exclusively at optical wavelengths, for reasons that are partly practical, and partly motivated by theoretical calculations of the relative information content of different portions of stellar spectra[5]. The ability to combat stellar jitter in the NIR due to the wavelength dependency of stellar activity induced RV noise[1], and the increased flux thus higher S/N ratio of M-dwarfs at these wavelengths, WISDOM choose an extended wavelength coverage.

Throughput (>10% average, >15% peak excluding telescope and atmosphere): Because of WIYN's relatively

modest collecting area, we have worked to maximize system throughput. A key parameter for high efficiency is the wide entrance fiber of 1.2″ that is only made possible at this spectral resolution for a 3.5m telescope by the pupil slicer.

RV Stability and Calibration: The EPDS Level 1 program requirements stipulated that "a velocity precision of better than 50 cm/s, with a goal of 10 cm/s. (excluding astrophysical noise)" has to be achieved. Meeting this specification requires exquisite environmental control/stability, a well understood RV error budget, and a calibration system that is intrinsically better than the required RV stability.

2.INSTRUMENT DESCRIPTION

Just like many modern PRV spectrographs WISDOM consists of several, well defined, and physically separated subsystems (see Figure 1), such as: the telescope interface or Front End (see 2.1), a Fiber Link (section 2.2) connecting the Front End to the Spectrograph (detailed in 2.3) that is housed in a tightly controlled Thermal Environment (see 2.4) also consisting of a vacuum chamber to provide pressure control besides the thermal insulation, and a Calibration System (section 2.5). The instrument control (IC) software talks to each of these subsystems, and communicates towards the telescope control system (TCS) software. A data reduction pipeline that can provide quick-look results, which was a requirement of the EPDS proposal, is directly connected to the IC system as properly sampled and archived telemetry data is essential for data reduction at the sub-m/s RV precision level. Relevant telescope and instrument parameters are captured within the FITS headers, as well as in a verbose and continuous telemetry data stream, which all gets transferred to a data archive server run by the NASA Exoplanet Science Institute (NExScI) where final data reduction takes place by the PRV pipeline.

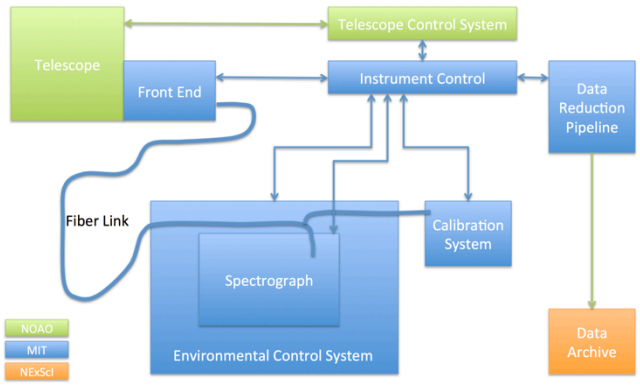

Figure 1. Major subsystems of the WISDOM instrument. Color-coding identifies responsible institutions.

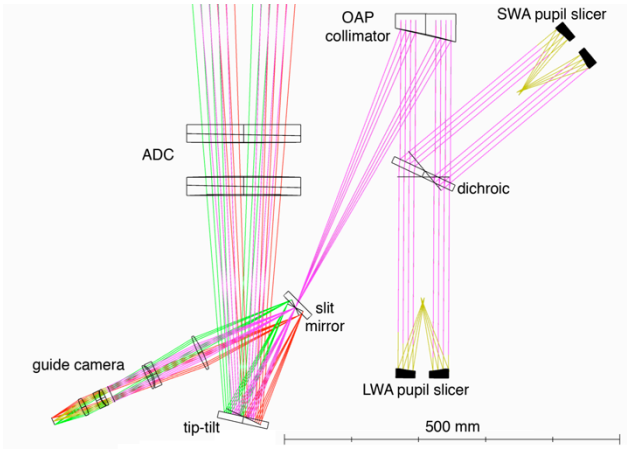

Figure 2. Optical layut of the WISDOM telescope interface.

2.1 Telescope Interface

The weight and moment limits of the telescope port necessitate a compact and lightweight Front End module. The large back focal distance (1 meter from the mounting flange) commands and provides a convenient path for a fold mirror, which has the dual purpose of reducing moment arm and staging the tip-tilt system (Figure 2). We considered multiple realization of this optical layout, settling on the L-bracket support structure and the arrangement shown in Figure 3. Because the port does not rotate, this configuration fixes the gravity vector in the plane of the major mounting surface where in-plane rigidity is highest. The cantilevered optics mounts present a bending moment of constant magnitude but changing direction to the mounting plate, however these again stay within the plane of highest stiffness.

Carbon fiber reinforced polymer (CFRP) is the optimal material for the Front End because of its low weight and high dimensional stability over the Front End's wide operating temperature range (-15 to +30°C). Depending on the resin composition CFRP boards can have very low (<1 ppm) or even nearly zero CTE. The associated opto-mechanical

components are kinematically mounted into cells, which interface to the CFRP structure via embedded titanium insert pads. Adjustable positioning blocks and shims achieve the relative alignment of the components.

We have engaged multiple CFRP vendors to further detail the design, performance and cost of such a Front End support structure. We provided these companies with a detailed weight and center of gravity (CG) location for all components, along with a list of positional and rotational tolerances derived from a Zemax image motion study (using ±0.1″ allowable tolerance as guide). Based on the preliminary analysis provided by the CFRP vendors all of our requirements for image stability are met by a ~70kg base support structure that brings the predicted overall Front End weight and moment to ~250 kg and ~1350 N-m, respectively (both including 25% margin), well within observatory requirements.

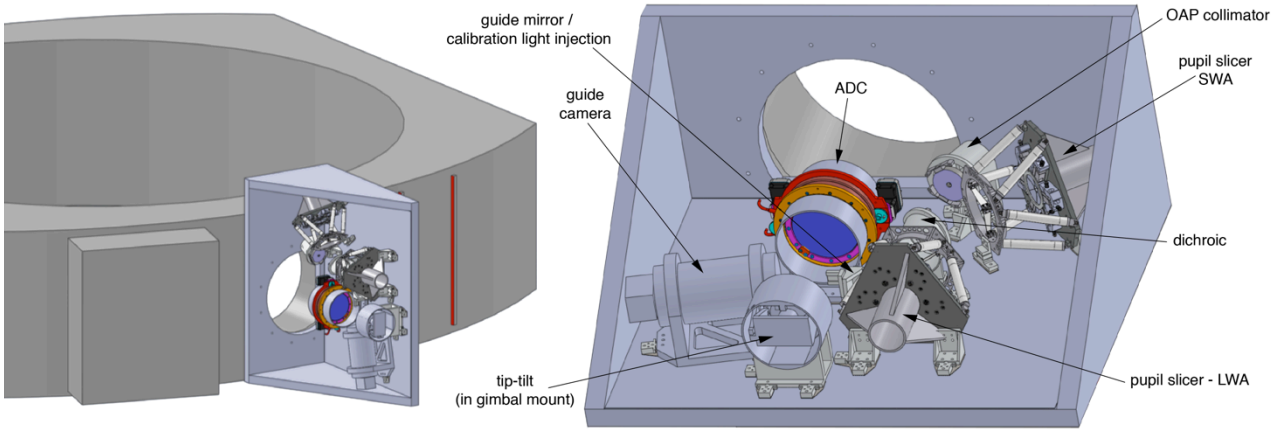

Figure 3. Opto-mechanical layout of the WISDOM Front End (right), and its relation to the primary mirror cell (left – the elevation axis of the telescope is running nearly horizontal from the 8 o'clock to 2 o'clock direction on that picture).

Front End Optical Design

Modern PRV fiber links utilizing non-circular fiber core geometries and double scramblers do a very good job at evening out illumination variations of both the fiber output (near field) as well as the spectrograph optics (far field). Both of these are typically induced by changes (guide error, atmospheric effects) at the coupling of telescope light into the fiber, and result in spurious instrumental RV signals, that can be as severe as tens of m/s. As described in the WISDOM fiber link paper[7] we did follow best practices in our design to mitigate such error sources, and while the NASA AO call did not require the proposing teams to develop the telescope interface, we felt that it is still a critical and integral part of any PRV instrument aiming sub-m/s precision. And so we took responsibility for both the optical and opto-mechanical design concept, except for the guide camera optics.

Atmospheric Dispersion Compensator

With WISDOM wavelength coverage from 380-1300nm it is somewhat challenging to design an ADC that provides a residual chromatic spread of <0.2″ over the 0-60° zenith distance range, but we found a solution using readily available glasses (Ohara S-FSL5Y and PBL6Y). It consists of two counter-rotating zero deviation prisms (Figure 4), with slight power that renders the effective focal length of the telescope to 21 m (F/6), providing a convenient 100 µm/1″ plate scale. The prisms are continuous RTV bonded into aluminum bezels and driven by stepper motors. The 510 mm back focal distance (BFD) provides adequate room for the fold mirror and guider assemblies.

Tip-Tilt Mirror

The fast-steering mirror design is driven by competing requirements on servo bandwidth, unvignetted field of view, and angular throw. The desire for high bandwidth and unvignetted guide field argue for locating the mirror close to the telescope's focal plane, because this minimizes its size and mass. But such configurations shorten the lever arm between the mirror and focal plane, increasing the piezo tilt (typically a few mrad maximum for COTS stages) required to achieve a given projected offset on the sky in arcseconds. We found an optimal BFD for the tip-tilt stage of 180 mm, this requires a ±3.4 mrad optical angular throw to achieve the desired ±5 times the 1.2″ (=120 µm) fiber aperture, translating to ±0.6 mm movement at focus.. Accounting for the 155° beam tilt, a 100 mm diameter mirror at this location transmits an unvignetted

6′ x 6′ FOV for a weight in Zerodur of ~200 grams. This mass/size can be accommodated by an nPoint RXY3-410 stage which has 4 mrad mechanical throw (±7.2″ on sky, 6-times the aperture size) in a compact package. Integral strain gauges permit closed loop operation with 0.2 μrad step resolution (0.0002″ on-sky) – far below the 0.7″ median seeing. With the aforementioned load estimate the 1st harmonic of the stage is about 300 Hz and settling time is <5 ms, which makes up to 100 Hz operation feasible.

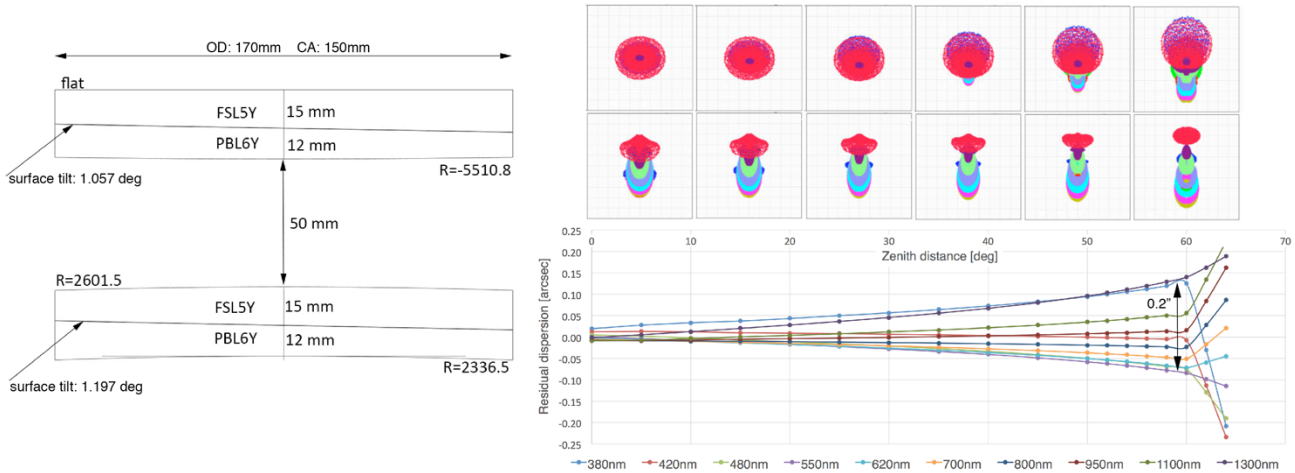

Figure 4. Optical layout (left) and performance of the ADC: spot diagrams (upper right, for 0, 15, 30, 40, 50 and 60° zenith distances, on axis and 3' off-axis) and residual color (lower right) as function of airmass. Box size is 0.6″ for the spots, half the diameter of the fiber aperture.

Guide Camera

Since our chosen fiber aperture, providing high throughput, is significantly larger than the median seeing, thus annular guiding is only possible for the brightest targets and/or in not ideal seeing conditions. The important question in the guide camera design is therefore the required field of view (FoV) that can provide a suitable guide star enabling the RV error budget imposed a σ=0.1″ guide accuracy requirement. The guide sources must be bright enough to close the tip-tilt feedback loop at a 10 Hz resonance seen in WIYN's telescope drives. This implies a 20-30 Hz bandwidth for the guide camera, which, after accounting for readout time, limits integration times to ~0.02 s. In general, centroiding accuracy of a guide star scales as the ratio of the width of the stellar profile to its signal-to-noise level: $\sigma_{guide}=\sigma_{PSF}/SNR$[8]; for WIYN's seeing of σ_{PSF} = 0.7″/2.3 =0.3″ we therefore target SNR > 10 for stars in the guide image (yielding σ_{guide} = 0.03″).

With these constraints, following a framework prepared by Jeff Crane for the G-CELF instrument, we estimated the guider FOV needed to present one guide star besides the target, observable at SNR=10 for exposure times ranging from 0.02 to 5s. We considered several different guide cameras and their characteristics (QE, read noise, dark current, sampling), and accounted for the optical train's throughput (including a 450-700 nm filter to ease the guide camera optical design), the atmosphere, sky background, and spectral energy distribution of the potential guide star. We made two independent calculations for different assumptions about the sky distribution of science targets. Our first simulation uses the actual *TESS* target catalog as a representative science sample, while the background field is drawn from the USNO-B catalog. The other assumes a worst-case configuration, simulating all targets and background stars based on galactic population model (Besancon models[9]) stellar field in the lowest density 10 square degree patch at the galactic pole.

Figure 5 summarizes the key result: a 4′x4′ FoV yields >90% probability of a guide star for both simulations, with rapidly diminishing returns at larger FoV. The pessimistic model performs less well for small FoV values, as expected. Allowing for annulus guiding for brighter stars, this FoV provides a reasonable expectation of 95% sky coverage at 0.02 s in the pessimistically simulated data.

Pupil Slicer

High spectral resolution is the most important feature of precise Doppler instruments, but diffraction theory dictates that resolving power scales with instrument size, so large instruments have accordingly large complexity and cost. For a telescope of fixed aperture D_{tel} and characteristic slit width φ matched to the site seeing, a spectrometer delivers fixed resolution at Littrow:

$$R = \frac{2D_{beam} \tan\delta}{\phi D_{tel}} \quad (1)$$

The value of R flows from scientific requirements (see section 1.2, 1.3), and the blaze angle δ is restricted by grating availability. Hence the collimated beam diameter D_{beam} (which drives instrument size) is essentially specified. For the median site seeing of 0.7″ and a typical echelle blaze of tanδ = 4, a 170mm diameter beam would be needed to meet our requirement of R=110,000 in such a conventional design. For improved throughput it is also desirable to increase the slit width, but for our goal of φ=1.2″ the spectrometer would need to be an additional 70% larger if maintaining the R=110k resolution. Project costs scale strongly with beam size and such a design would be difficult to fit within the space constraints of the designated spectrograph room at WIYN. More on the implementation of the pupil slicer can be found in [7] and [10], here we just point out that with a 6-way slicing of the pupil we managed to reach the R=110k target resolution for the 1.2″ fiber size with a 125mm beam. (HARPS has a 200mm beam for similar R and D_{tel}, while for a smaller aperture of φ=1.0″.)

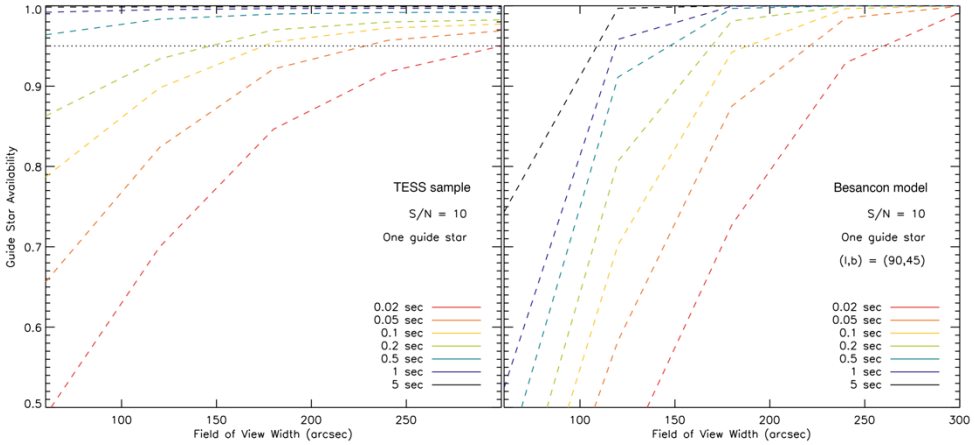

Figure 5: Results of our guide star availability calculations. The left figure is based on nearest star search in the USNO B1.0 catalog for an actual *TESS* target list containing 210,000 stars. The right panel is for a simulated stellar field at the galactic pole, using the Besancon models. Curves are plotted for different exposure times.

2.2 Fiber Link

The pupil slicer feeds 6 identical, 32μm core octagonal fibers. The non-circular core geometry inherently increases the near field scrambling or in other words the stability of intensity distribution as seen on the fiber output face. Changes of the near field would directly map into spectral line profile variations since every spectral line is essentially a monochromatic image of the fiber output. Near field variations are induced by changes of light coupling into the fiber due to guiding errors and atmospheric variations, and use of octagonal fibers allow for a relatively relaxed requirement of ±0.2″ on the guiding.

Spectral line variations can also be a consequence of illumination variation across the spectrograph pupil, or as it is referred to the far field. Stronger illumination at the edge of lens elements weigh aberrations more heavily into the point spread function (PSF) of the optics, and this could, in a complex and wavelength dependent way, affect the line centroids and thus result in instrumental RV errors. Since fibers, even non-circular core ones, do not scramble the far field sufficiently, a single ball-lens based optical double scrambler[11] is employed in the WISDOM fiber run.

The small core diameter fibers, especially considering the long wavelength NIR channel of WISDOM, only support about ~80 light propagation modes above 1μm. This results in a very strong modal (interference) pattern at the fiber output end face, that changes over time but in a way that the photometric centroid might be not consistent between measurements. To combat this modal noise that can severely affect the near field and thus line centroids, we combine 3-3 fibers into 3:1 elongated rectangular fibers with a larger modal area, which form the spectrograph slit. In our design we also actively mitigate modal noise by physically agitating part of the fiber link. More details of the fiber link design can be found in a separate, dedicated paper [7, these proceedings].

2.3 Spectrographs

The WISDOM optical layout follows the asymmetric white pupil arrangement that is often the choice for PRV spectrographs. The white pupil means that the illumination of the camera optics is very similar at all wavelengths, and thus

optical aberrations and time-dependent spectral line profile variations are very much the same across the entire echelle passband. This minimizes systematic instrumental RV errors, while also allows for small camera optics, especially with higher level of asymmetry in the pupil relay like the 2:1 ratio applied for WISDOM. The optical design and its considerations are described in detail by a dedicated paper [12, these proceedings], and so here we just very briefly summarize the optics and rather concentrate on the opto-mechanics.

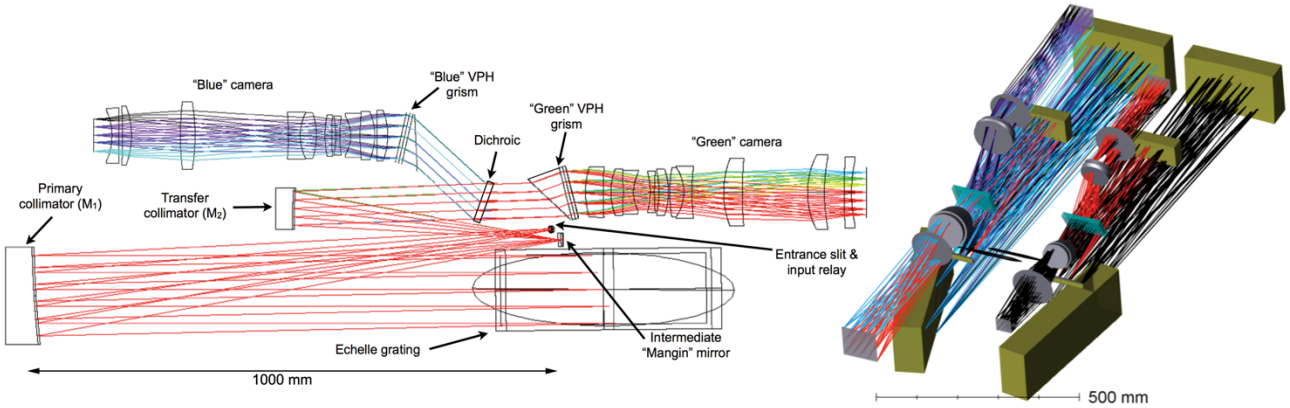

Figure 6: WISDOM has the typical asymmetric white pupil layout of a modern PRV instrument (left). Since there are actually two spectrographs these can be arranged in a mirrored symmetry, that results in a very compact instrument (right).

Optical Bench

As shown on Figure 2 the Front End splits the collimated beam to a short and long wavelength arm (SWA: 380-750nm; LWA: 750-1300nm) before the pupil slicer and fiber feed. The two sets of fibers run into two separate spectrographs, each following very similar asymmetric white pupil layouts as the one shown on the left of Figure 6, for the SWA. Each spectrograph has two cameras, with their optical axis folded by the dichroic and cross-disperser grisms to be parallel to the optical axis of the white pupil relay. This results in a planar, elongated, very compact package with the actual fiber input folded perpendicular to the main plane. Given the high level of similarity between the SWA and LWA spectrographs and their planar arrangement, it comes naturally to arrange them next to each other by mirroring the components to a vertical plane, as shown on the right of Figure 6. Such arrangement results in a very compact instrument volume, and allows for a very simple, rectangular, planar optical bench placed at the center. Each optical component then is mounted via cantilevered supports on either side of the bench, effectively cancelling out any bending moments (Figure 7). Therefore the load is entirely within the plane of the bottom-edge supported vertical bench, utilizing its maximal possible stiffness and bearing capacity. Further advantages of this layout are the straightforward kinematic support of such bench, as well as the decreased sensitivity to environmental temperature gradients that naturally develop vertically due to gravity (as discussed in section 2.4).

The bench rests inside the vacuum chamber on two kinematic supports (ball-cone-groove) located on its long edge with a third constraint on the top to plumb the vertical (see Figure 7). These interfaces transmit zero stress into the bench from the vessel walls (which can deform under atmospheric pressure load), and have small contact patches to minimize conductive path from the dewar vessel into the bench.

We contracted a customized conceptual design of a CFRP bench from CarbonVision GmbH, to simple rectangular dimensions of 1700 x 600 mm and 90 mm thickness. The face sheets are 10mm thick laminated plates, but the bottom edge (which supports the spectrograph weight) uses a 20mm laminate. The carbon fiber has very low coefficient of thermal expansion (CTE, typically $\lesssim$1ppm) and high strength, providing the required thermo-elastic stability for WISDOM's optical components. The face sheets are reinforced by a grid of connecting carbon fiber tubes for rigidity in the perpendicular direction. These connections are important not just for structural but thermal reasons as well, since the CFRP plates only have low CTE in the direction of the fibers and not perpendicular to the plane of the laminates. Latter is mostly affected by the relatively large CTE of the resin, so connecting the faceplates of the bench with CFRP tubes increases thermal stability across the thickness of the bench. Still, components should not be directly mounted on the surface of the faceplates, as the thermal expansion of the resin could "lift" the parts, and do so unevenly, as resin properties might not be homogenous across the faceplate. Therefore post-machined Titanium inserts are integrated into the CFRP face plates during their manufacturing, to provide mounting references and alignment indices for opto-mechanical components.

According to the vendor quote, based on a detailed analysis of the bench structure, the price is very competitive compared to other low CTE or more conventional options we investigated (zerodur, invar, aluminum and steel bench structures). While the weight was not a primary concern in our application it is certainly highly advantageous from the handling point of

view. The only concern is outgassing as CFRP is known to be hygroscopic, and so ultimate dimensional stability within a vacuum enclosure is only reached after the bench "dries out". Based on test data collected by the vendor during space qualification of their CFRP plates we estimated that our bench would reach a stable state within a couple weeks. Since PRV instruments are typically operated undisturbed for long periods of time once the vacuum enclosure is closed, we decided such initial settling period does not affect our ability to commission and then operate the instrument on the long term.

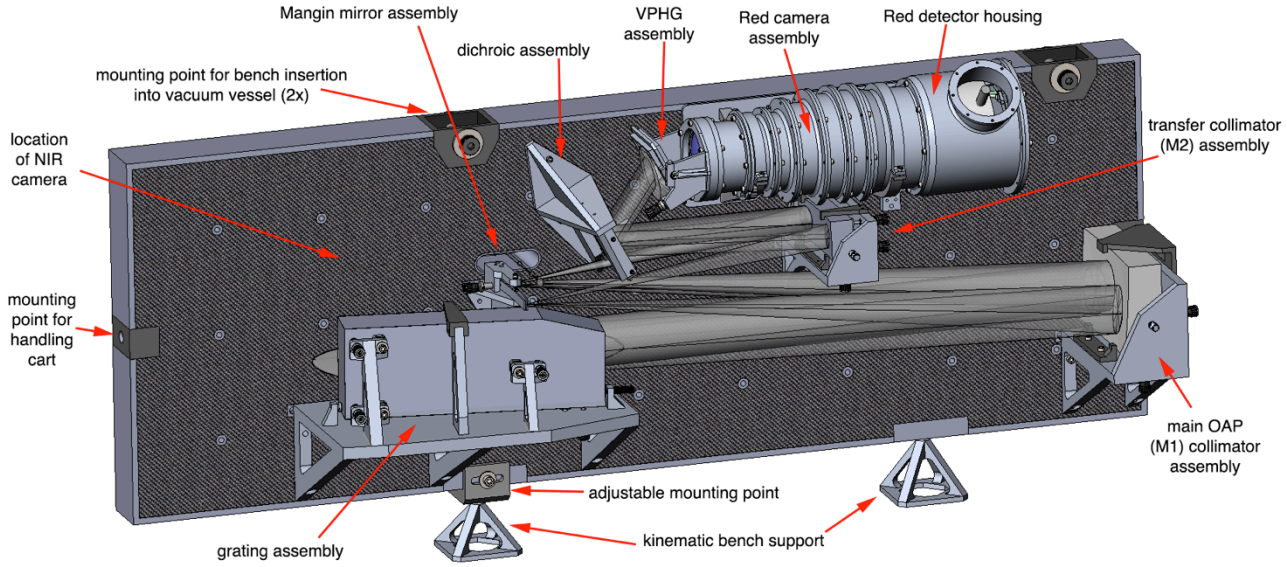

Figure 7. Solid model of the CFRP optical bench and opto-mechanical LWA assemblies. For simplicity, only the Red channel is depicted and the NIR camera is not shown. An identical layout is on the reverse side of the bench for the SWA.

Opto-mechanical Assemblies

The Level 1 Program Requirement of <0.5m/s RV precision corresponds to a <2nm (0.0001 pixel) physical shift of the spectrum on the detector. This flows down to thermo-elastic stability requirements between the slit, the detector, and any other optical components not in the collimated beam. For the focal lengths employed in WISDOM's design, it also implies <0.001″ tip-tilt stability for the individual optical components, similar to other PRV instruments. Given the complexity of the instrument (and the mission-driven timeline and budget of the project) it is impractical to build such a high fidelity and complex FEA model that demonstrates absolute stability at this level. It is inevitable that components will see displacements of 2nm/0.001". The goal is therefore not to eliminate such motions, but rather to lengthen their timescale so that their signature in the data may be removed through calibration.

Cross-correlation techniques can track internal changes of a high resolution echelle spectrograph at the <0.1m/s level using proper calibration frames. In this way, *common mode changes* between the science and calibration exposures can be calibrated out at the 0.1 m/s level, leading to the following philosophy for opto-mechanical component design:

a. Maintain constant pressure, gravity, vibration isolation, and multi-layer thermal control in conjunction with kinematic mountings to minimize time-dependent opto-mechanical displacements
b. Maximize the thermal time constant of the system;
c. Leverage the low CTE (<1ppm/°C) and dimensional stability of the CFRP optical bench;
d. Enforce material homogeneity for opto-mechanical mounts and avoid over-constraining.

Each optical component is directly referenced to the CFRP bench, so the actual optical mounts need not be made out of zero-CTE materials. This saves weight, but more importantly cost. Precision tooling balls are pressed into the optics mounts and received by precision bored holes/slots embedded into the bench, ensuring that differential thermal expansion between the bench and the mounts do not change the spatial and/or angular alignments.

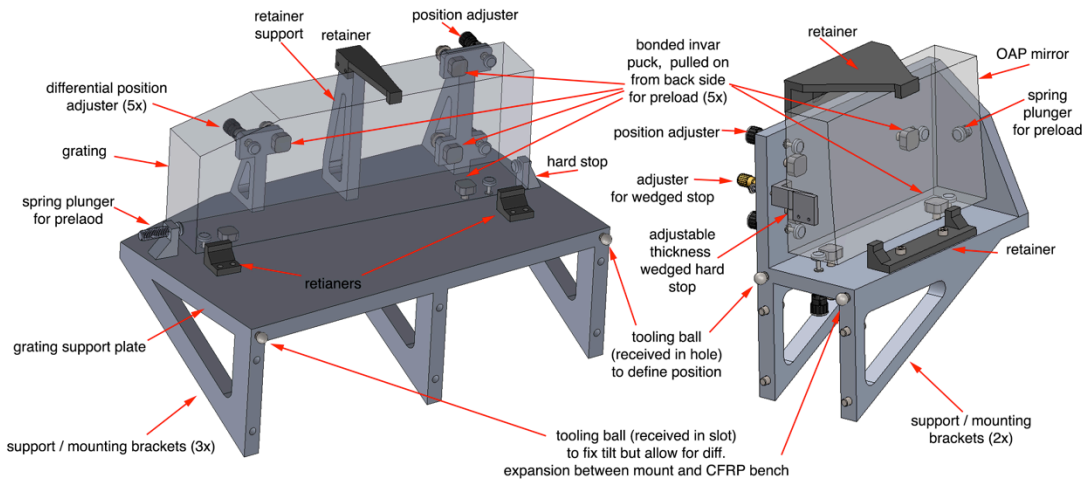

Figure 8. Representative optical mounts for the grating (left) and M1 OAP collimator (right)

There are two basic type of optics mounts: the ones in collimated beam (grating, dichroic, VPH) that are sensitive for tip-tilt tolerances only, and the others in converging/diverging beams (slit and pre-optics, M1, M2, Mangin fold, cameras) which are sensitive to both lateral and angular misalignments. The former ones are mounted on 7075 alloy aluminum structures, as in parallel beam the very small lateral displacements due to the higher CTE of the mounts (~24 ppm/°C * 0.001° C * ~150 mm = 4 nm) do not effect RV values. The rest of the optics are either pre-loaded against the CF face sheet of the bench (slit, M1, M2) or cantilevered on Invar supports (Mangin mirror, cameras). See Figures 8 and 9 as representative examples.

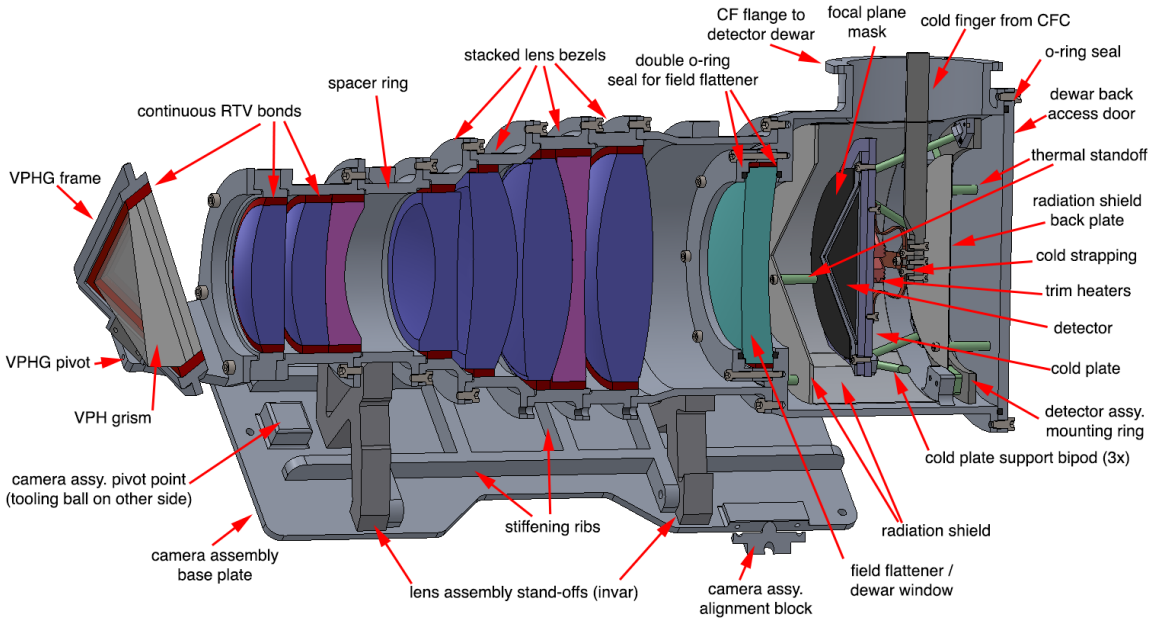

Figure 9. Details of the camera assembly represented by the Red camera in a cross section/cutaway view

The camera lenses are potted into aluminum 7075 bezels by a continuous RTV bond. In this application the thickness and shape factor of the RTV does not have to be tweaked for athermalization, thus we select a bond geometry that minimizes gravity induced sag of the lens within the bezel while still allowing for easy injection of the silicon based adhesive. Bonding is done in a custom alignment fixture, unique to each lens. This ensures alignment of concentricity and tilt between the lens and the bezel, thus transferring the optical references to mechanical ones. Each bezel features precision machined alignment rims for stacking them up and bolting together into the final camera lens assembly. Each camera assembly can be tip-tilted around a tooling-ball defined pivot point under the first lens element, by shimming against the bench face plate and rotated by shimming against an alignment block that is attached to the bench. This is similar to the dichroic or Mangin mounts.

The detector heads inhabit vacuum volumes distinct from the main chamber. They attach directly to the lens assembly, and have three ports. The front port integrates the last lens of the camera, which acts as both a field flatter and a dewar window. This lens is also bonded into a metallic bezel but it has an O-ring seal on both faces side, so it can alternate pressure differential between the vacuum vessel and the detector housing (which can happen during assembly, integration, and test or in the event of a leak in a detector head). The back side presents an access port through which the detector assembly can be inserted to the head, and affixed to cold strapping and wiring. The detector itself is attached to a cold plate, made out of SiAl alloy (CE6) for CTE match to the detector packages. The cold plate attaches to a mounting ring via three carbon fiber bipods, minimizing conductive coupling to the detector stage. The cold plate also hosts a heating element and an RTD sensor, which allows for few mK level thermal stabilization of the detector. The third opening in the detector head accommodates the incoming cold finger and associated bellows and radiation shield, described below in section 2.4.

2.4 Environmental Control

Vacuum vessel

WISDOM's compact layout permits packaging within a standard cylindrical vacuum chamber, which simplifies design of the thermal control system and lowers cost. We have selected Kurt J. Lesker for chamber manufacture who offers stainless steel COTS cylindrical vessels in diameters up to 950 mm that can be cut to specified length and fitted with conflat flange (CF) ports to customer-specified prints (see Figure 10). The WISDOM vessel has 13 CF ports, and both ends of the cylinder are fitted with full-diameter hinged doors sealed with o-rings. The doors are opened for insertion of the bench and connection of the camera heads' electrical and thermal feeds. Two 16 inch access ports on opposite sides of the vessel midpoint facilitate in-situ inspection and optical alignment, installation of the slit mechanism, and house the fiber optic and electrical feed-throughs. A vertical central port services the pumping station with a large ion pump and separate turbo station. Dual gate valves are arranged in a configuration that allows direct turbo pumping on the science dewar (post-servicing), ion pumping alone on the main dewar (during normal operations), and full isolation of the dewar for regeneration of the ion pump by the turbo pump in conjunction with an integral heater. The ion pump is sized to maintain $<10^{-6}$ mbar vessel pressure over a several day period. The turbo pump station is connected via a force-free bellows system for vibration isolation; the design takes up compression of the bellows under vacuum without imparting force either to the vessel or the turbo station. The turbo station is supported outside the thermal enclosure on a dedicated vibration isolator. The four remaining vacuum ports accommodate the detectors, offset 45° from the vertical mid-plane of the chamber.

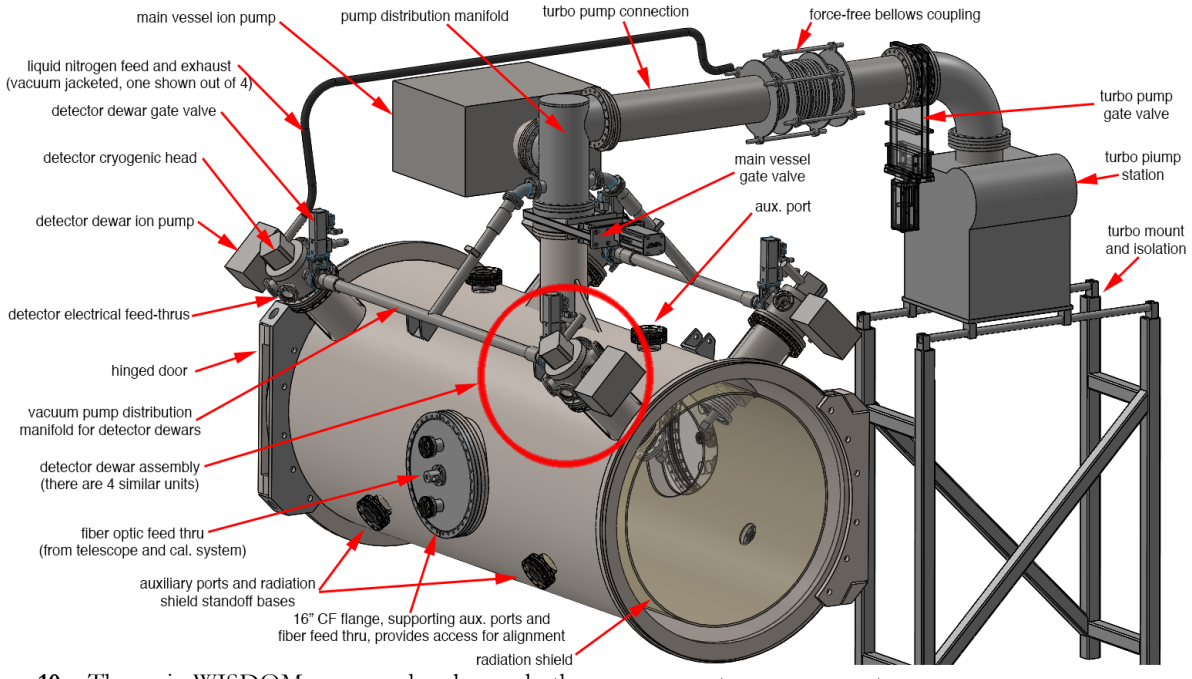

Figure 10. The main WISDOM vacuum chamber and other vacuum system components

Detector dewars

The detector dewars bolt to the main chamber, which presents exterior weldments 200mm in length, terminated with 8" CF flanges. The dewars' main assembly is a short cylindrical adapter that mates to the main chamber on one side, and a continuous flow LN2 cryostat (described below) on the other. The adapter includes additional flanges to accommodate: a) a pneumatic gate valve connecting the dewar individually to the vacuum manifold (in common path with the main vertical pumping port); b) a small ion pump that maintains operational pressure at 10^{-7}mbar; c) detector electronics, housed just outside the vessel; and d) other electrical housekeeping lines. The dewar adapters are assembled and integrated externally, with the cryogenic head attached last.

Ultra-precise temperature control at the detector is critical for PRV applications. We have selected a continuous flow cryostat (CFC) custom engineered by Janis that has achieved mK stability at -110°C for thermal loads of several W. We prefer liquid nitrogen systems to mechanical chillers, because of their lower vibration and robustness to power outage. The projected LN2 consumption rate is 0.25l/hr/dewar, or <25 liters per day for the entire instrument.

Electrical harnesses and the cold finger penetrate the main vessel within a 6" tube with integrated radiation shield. The inner end of this tube is welded to a small bellows, which is in turn flanged to the detector housing on the optical bench. This arrangement takes up small alignment offsets between the dewar port on the chamber exterior, and the detector head on the optical bench. It also mechanically de-couples the two systems subject to the spring constant of the bellows. By selecting a thin/finely structured bellows, and maintaining only a small pressure difference between its two sides (10^{-7} vs. 10^{-6}mbar), dynamic and thermal coupling between the vessel and the bench is minimized.

Thermal and vibration isolation

The chamber is supported in suspension, to lengthen the conductive path between the floor and the optical bench. There are two I-beams over the main vessel, which are mounted on stainless steel pedestals with a passive vibration isolator on top of those stands (see Figure 11). This way the thermal path to the ground goes from the bottom of the vessel, that kinematically supports the bench with a very small contact patch, all the way around the vessel, through the thin cross-section suspending blades, the I-beams, the insulators and then the pedestals. Since the ground presents a huge thermal mass that is impossible to control, this increased thermal path is highly advantageous. To combat any parasitic heat loss to the ground each suspension blade will be wrapped with heater tape and insulation, and a PID control loop will maintain its temperature at the 20°C set point of the chamber. (More on the active temperature control is discussed below).

The I-beams are positioned so they clear the dewar assemblies, but also provide support against the weight of the ion pump and gate valve assemblies. The beams themselves are resting on tuned damping passive vibration isolation platforms. These units are provided by the company Minus K, have more than adequate load capacity and their damping properties will be tuned to the final mass and geometry of the overall WISDOM spectrograph assembly.

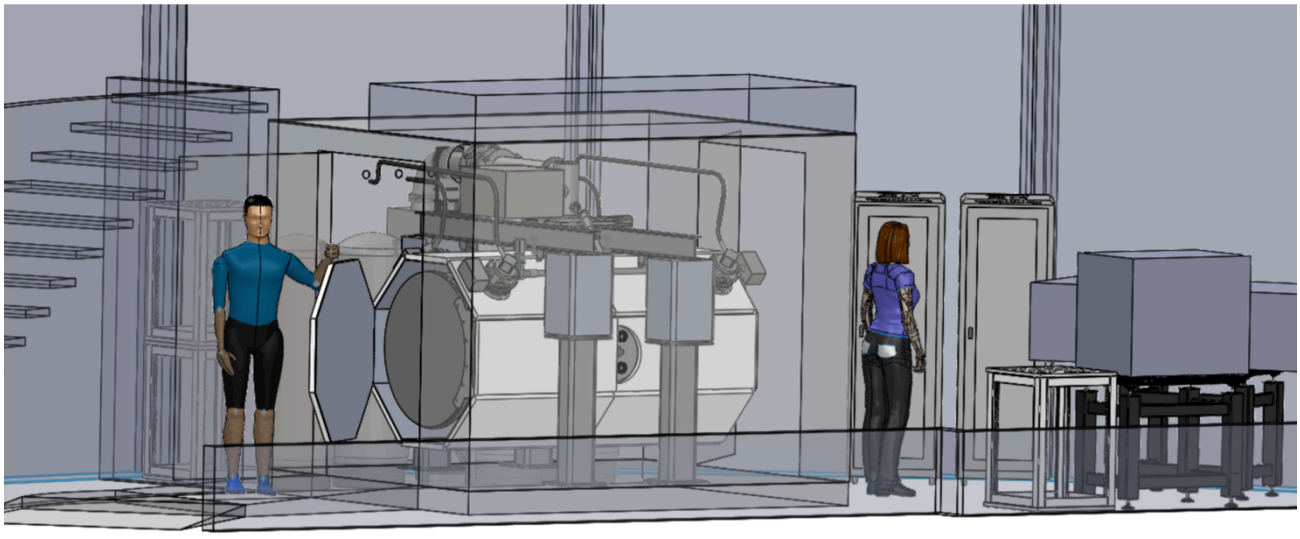

Figure 11. The WISDOM cold enclosure, shown within the spectrograph room, contains the spectrograph. Turbo pump station and the LN2 dewars are under the staircase, behind the cold enclosure. The vibration isolation stands and I-beam suspension beams are visible, and the vacuum vessel is enclosed in its white, octagonal, multi-panel thermal control shroud. Calibration system bench is shown at right with electronics racks of the instrument.

Thermal control system

The advantage of the vertical optical bench is that the main dispersion direction of the echelle gratings is then horizontal. A vertical temperature gradient therefore, which naturally builds up in the environment due to gravity, would imply a thermal bending of the bench that moves the echellogram only in the cross dispersion direction (up-down), and therefore not cause a systematic RV error (equivalent of sideway displacement of the spectrum). Placing the spectrograph in vacuum and enclosing it within a tightly controlled heating shroud reduces the sensitivity to such temperature gradients and its variation in the surrounding air/environment.

There is still, however, a conductive path along which gradients can develop, since the bench needs to be supported or suspended within the vacuum enclosure. Minimizing the efficiency of such conductive pathways to ground (by maximizing its path and actively controlling it, as described above) is just the first step in achieving exquisite thermal control. Since the spectrograph room only offers ±5C° temperature stability, additional layers are needed between this and the WISDOM vacuum vessel. We will surround the instrument with a 8 x 10 x 8 ft COTS, modular refrigerator room, offered by MasterBuilt, that has 6 inch foam insulated walls sandwiched between steel panels. This room will have a commercial indoor air conditioning (AC) system, utilizing the chilled water supply provided by the observatory, to maintain a better stabilized (±1 °C) immediate environment to the vacuum chamber. With the AC set to maintain a 17°C air temperature and heating the chamber to 20 °C there will be a constant, uni-directional heat flow from the instrument to the air of the cold room. Fully circulating the air every minute (a modest 640 cfm flow) any of the internally generated heat can be extracted efficiently.

The vacuum chamber will be warmed by a modular, multi panel heating enclosure (Figure 11). These panels symmetrically surround the vessel, divided into 8 radial x 2 axial segments, plus end panels - totaling 18 zones. This allows control of any gradients, radial or axial. Each panel consists of a 3mm thick aluminum heater plate that quickly and evenly distributes the heat provided by several optimally located thermal tapes. To prevent cross talk of the panels, and to insulate them from the significantly varying air temperature of the cold room, the panels are insulated from each other and to the ambient air.

The heater panels will have a set point of 20°C, with expected variations of <50 mK using simple PI control loops. To achieve this while maintaining constant outward heat flow, the panel exteriors must be insulated. Balancing the time constant of this insulation is critical for the competing desires of thermal isolation and controller response. Analytical calculations and numerical simulations show (Figure 12) that for a given period and amplitude of air temperature swings in the cold room, an optimal insulation thickness can be found (in our case 30mm), allowing for the AC-induced variation to penetrate only 2/3 into the insulation but not all the way down to the panels (Figure 12, left).

Relying on the slow convective coupling to the vessel through air trapped in the octagonal box, the large thermal inertia of the vessel itself, and then the long time constant of radiative coupling to the bench further smoothed and lengthened by the radiation shield, we expect the temperature of the optics to float at the heater set point of 20°C but with a precision of <±0.001°C.

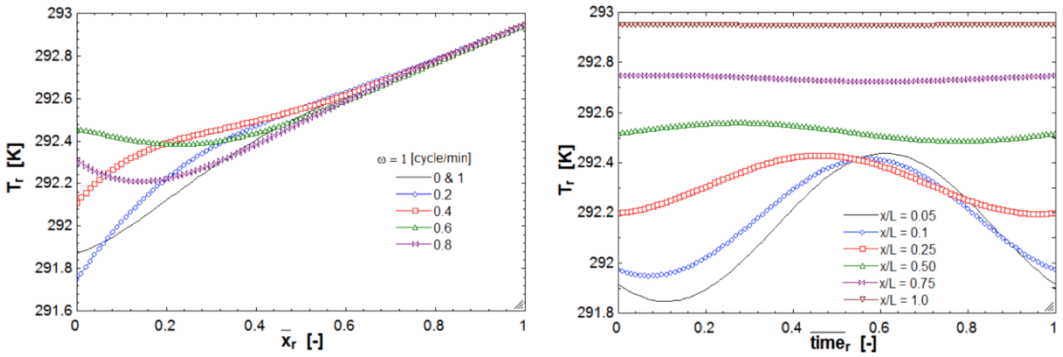

Figure 12. Penetration of the 17±1°C air temperature variations into the insulation of the heating panels (set at 20°C), shown at different phases of the AC oscillation (left), displayed as a function of dimensionless (normalized) thickness. The right panel displays the temperature variations as a function of time at certain normalized depths, where time is also normalized to the cycle interval (phase plot).

2.5 Calibration System

The laser frequency comb (LFC) and ThAr lamp wavelength calibrators, along with light sources for flat-fielding (Energetiq LDSL XC) and the input from a solar telescope[13] will be fed into a calibration multiplexer. This optical selector stage can inject any single input (or combination of them) into: a) the science fibers, via a fiber optic link that directly runs up

to the pupil slicer (at the telescope Front End) from the calibration system; b) into a dedicated simultaneous calibration fiber that runs directly into the spectrograph, positioned in between the two 3:1 rectangular fibers of the slit assembly[7]. Part of the optical selector/multiplexer is a pair of neutral density filter wheels that allow for SNR matching between the light of the science and simultaneous calibration fibers.

At the telescope Front End, a set of optics converts the calibration fiber output into a diverging F/6 cone that matches the WIYN+ADC focal ratio. An observer-controlled sliding fold mirror blocks starlight from the telescope, just past the aperture/slit mirror assembly. This mirror redirects pre-conditioned calibration light into the pupil slicers; calibration light then travels through the exact same path within the WISDOM instrument as starlight does. This allows for observing of calibration data that carries as similar instrumental imprints to the starlight as possible.

The LFC is made by MenloSystems, and it is based on an ytterbium (Yb) fiber laser oscillating at a wavelength of 1.04 microns with a pulse repetition rate of 250 MHz. This creates a series of individual "teeth" whose absolute optical frequencies are spaced by 250 MHz (≈1 pm at 1 μm) and known to a fractional precision *and* accuracy of 1 mm/s in radial velocity. This "source" comb has a native resolution of R~1,000,000 and is therefore unresolved by WISDOM, and it only spans a modest wavelength range near 1 micron. To reduce the spectral density to appropriate levels, light from the source laser comb is filtered in a series of Fabry-Perot cavities to a spacing of 18 GHz, transmitting only one out of every 72 orders. After filtering, the LFC light traverses a series of optical fiber amplifiers and is broadened in nonlinear optical fiber via a mixing process to produce calibration lines from 420nm to 1.3 microns, in parallel blue (420-750 nm) and red (750-1300nm) arms that are then recombined with a dichroic beam splitter before entering the calibration multiplexer.

In wavelength regions not covered by the frequency comb – especially the UV and IR ends of WISDOM's passband – a secondary calibrator is needed. We will use a thorium lamp for such coverage. While high quality metal thorium lamps are currently difficult to acquire, oxide lamps will provide sufficient precision when referenced to the primary calibrator across the large range of wavelengths for which they overlap.

The solar telescope[13] consists of a 76 mm achromatic lens, which feeds an integrating sphere to scramble the solar disk, all held on an amateur telescope tracking-mount. The integrating sphere couples to a 100 micron core optical fiber which is fed to the calibration multiplexer. To allow for robust, unattended operation, the telescope is placed under a fixed, transparent acrylic dome. Such solar telescope is already installed at HARPS-N by our group and routinely realizes radial velocity sensitivity of 30 cm/s RMS, near photon shot-noise limited performance.

3.PERFORMANCE PREDICTION

3.1 Throughput

The spectral throughput budget is tracked for each of the four arms of the spectrograph (Blue, Green, Red, NIR). We account for reflectance and transmittance at every surface and boundary, including transmission through glass elements, surface coatings, Echelle and VPH gratings, and geometric factors. Through an early contract for initial coating definitions with the company Evaporated Coatings, Inc. (ECI), we obtained reliable coating estimates for all of the coated surfaces, which provides for a high degree of confidence in the surface coating values. The cumulative throughput fraction as light travels through the system, starting with the atmosphere and arriving at the detector, is illustrated in Figure 13 for the Green arm. The most significant contributions to throughput loss occur at each of the WIYN telescope mirrors (90-92% efficiency), the slit loss (~61% efficiency), and the Echelle geometric loss and blaze efficiency (~56-62% efficiency)

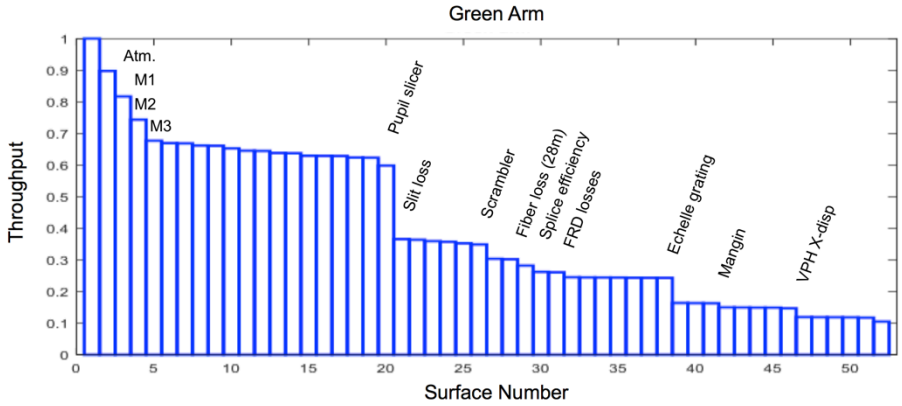

Figure 13. Stackup of throughput loss by surface number

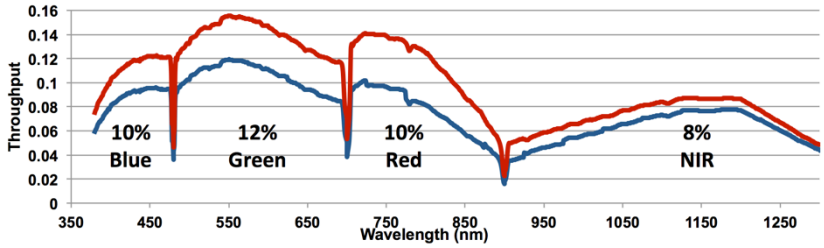

Figure 14. Total throughput model, absent echelle blaze efficiency variations within spectral orders. The red curve represents the entire WISDOM instrument (front end, slit loss, fiber link, spectrograph, detectors), while the blue curve also adds in the WIYN telescope and the atmosphere at Kitt Peak.

The total spectral throughput as a function of wavelength is shown in Figure 14. The peak efficiency, including atmosphere, telescope, front end, slit loss, fiber link, spectrograph and detector, is 12%; the mean is 8% across 380-1300 nm, while it is 9% for the optical channels (380-900 nm). For comparison, the peak for HARPS efficiency[14] is ~6%, leaving WISDOM a substantial advantage and making it one of (if not) the most efficient fiber-fed PRV instrument. This is due to the fact that the overall instrument passband is broken into fairly narrow wavelength segments amongst the 4 cameras, which allows to optimally utilize the high but not broad efficiency of VPH gratings, as well as the use of highly efficient anti-reflection and mirror coatings.

3.2 Radial Velocity Error Budget

Framework

Figure 13 displays a framework for modeling WISDOM's RV error budget. This model, developed from [15] is used to: a) identify and control all known sources of noise that could threaten the 0.5m/s single measurement error (0.1m/s goal) Level 1 requirement; b) to provide a strategy to verify such performance; and c) to define pathways for verifying subsystems during AI&T. We interpret "RV single measurement instrument" error as the 1σ dispersion of a series of measurements over time, incorporating the contribution of instrumental errors only. This implies that the target under observation is noiseless and the reference spectrum against which the observed spectrum is cross-correlated is also free of errors.

Any study of potential error sources begins with a detailed understanding of the data reduction and RV calibration procedure. From these procedures, we generate an error budget that is organized into two main trunks: **non-calibratable instrumental errors** and the **post-calibration residual**. Non-calibratable errors affect the reproducibility of our wavelength fit or cross-correlation, and generally are comprised of random noise sources for which we have imperfect or no telemetry. We estimated the contribution of each of these sources from best practices, FEA modeling, or research, and added their full values in quadrature (RSS, root-sum-square) to the total single measurement instrumental error.

Some fraction of non-calibratable errors can in fact be traced back to systematic drifts in the instrument, provided that post-commissioning plans include rigorous long-term monitoring of quiet targets with low astrophysical noise. A single commissioning run does not provide sufficient baseline in any dimension to reveal unforeseen correlations between instrument telemetry and drifting RVs of benchmark stars.

Calibratable errors encompass variables that affect RV performance, but which can be measured during AI&T or telemetered during operations, and then regressed and removed from the data. This process substantially improves RV performance but the fitting process does leave residuals that flow into the single-measurement error budget. The precision penalty of post-calibration corrections scales with the size of the signal being de-trended; in general the pipelines correct to within a few percent of the signal. To be conservative, we adopt a 20% residual post-calibration for common path instrument errors. The contribution to the total budget is therefore calculated by estimating each correction size from analysis, and RSS summing 20% of that value with the non-calibratable errors. We also reserve a sizable margin (0.25m/s) called out explicitly in the error budget.

Non-calibratable instrument errors are counted once in our single measurement error budget, assuming that the reference spectrum for cross-correlation is ideal. In practice, RV science measurements are differential in nature, in which case the diamond-shaped branch labeled "×1" (at the top of non-calibratable errors) would become "×1.4." Here a factor of $\sqrt{2}$ should be applied for realistic differential RV measurements, since the target spectrum is cross-correlated twice with the template (or against itself), and the non-calibratable errors therefore appear twice. During operations the RV error budget should include the factor of 1.4 for the use case of phasing stellar orbits. (For the presented framework we used a factor of 1, due to an explicit NASA requirement for verification of "single-measurement RV instrument error, absent astrophysical source noise".)

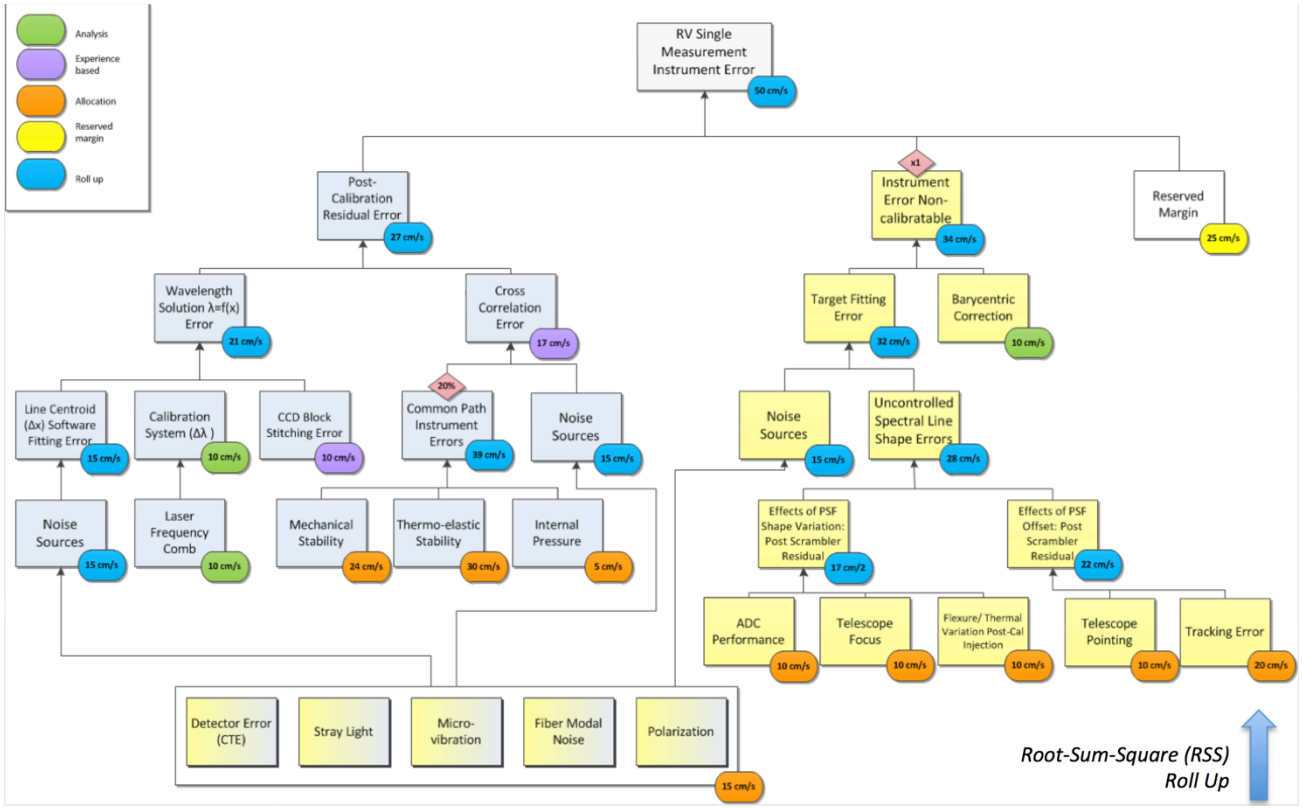

Figure 15. RV error budget tree: blue boxes indicate the terms contributing to the post-calibration residual, yellow boxes indicate the terms are non-calibratable instrument errors, and dual colored boxes show the terms contribute in different places on either branch. The brightly colored overlay boxes show the magnitude of the error term, color coded to indicate how the value is determined in the current error budget.

Definition of Individual Error Terms

We describe key terms in descending branches of RV error budget, working from left to right on the figure.

Post-Calibration Residuals:

Wavelength Solution Error: uncertainty in the fit of wavelength as a function of CCD pixel position. Within this term there are three contributions:

Line Centroid Software Fitting Error: uncertainty in the fitted pixel position of the spectral lines in the calibration spectrum, which is affected by Noise Sources that broaden these lines or add background noise contribute to degraded performance in the line fit.

Calibration System: precision of the wavelength reference position ($\Delta\lambda$) and the availability and spacing of reference lines. The LFC provides the fundamental limit on the calibration wavelength stability and effective line width.

CCD Block Stitching Error: uncertainty in the absolute CCD pixel position and spacing for adjacent sections of the chip; sections can have irregular spacing due to placement of the lithographic mask when forming the CCD.

Cross-Correlation Error reflects the width of the cross-correlation peak obtained after the science target has already been wavelength calibrated. There are two sub-contributions to this term:

Common Path Instrument Errors: these are terms which affect both calibration and star light. Since they generally vary slowly with respect to measurement cadence, they may be accommodated in calibration.

General Noise Sources: groups terms that contribute random or constant noise over time. Scattered light, or other features that reduce the SNR of the observed spectra are counted here. Mechanical or optical noise sources (micro-

vibration, CTE, fiber modal noise) introduce fit errors at different stages: in determining the wavelength solution, the calibration spectrum, and separately in fitting the target spectrum. These errors are non-calibratable, but introduce a limit to the accuracy of the calibration process. For this reason General Noise Sources are shown in the budget as contributing to both sides of the error tree.

Non-Calibratable Instrument Errors:

Target Fitting Error: reflects the uncertainties arising from mapping and extracting the correct stellar signal onto detector pixels.

Uncontrolled Spectral Line Shape Errors: change the line shape profile over position or time, causing the spectral line shape to shift, blur or otherwise vary. These allocations reflect post-scrambling residuals.

The systems that will affect the line shape include the ADC Performance, Telescope Focus, and Flexure or Thermal Variation Post-Calibration Injection. A systematic tracking or target acqusition error will cause the star image to shift relative to the fiber entry, which in turn causes changes in the near- and far field ilumination of the spectrograph, resulting spurious shifts in the spectra on the detectors. Factors that affect the line centroid position are counted in the Telescope Pointing and Tracking Errors.

Barycentric Correction Errors are associated with uncertainties in observatory location, stellar position and parallax, time of observation, and intensity variations during integration, which add directly into the RV measurement at the last step.

A complete description of the RV error budget is beyond the scope and page allocation of this paper, but to illustrate the procedure we describe an example of one such roll-up for the largest single source of error: the telescope tracking.

We calculate the RV allocation for tracking errors considering the maximum displacement on the input fiber, d, and calculating the attendant fractional shift in wavelength, f, compared to the FWHM of the spectral line profile, F. Using the fiber diameter D these define the scrambling gain[16]: $SG = (d/D) / (f/F)$. We equate the FWHM (F) with the wavelength differential $\Delta\lambda = \lambda/R$, corresponding to one resolution element. For λ=760 nm, R=110,000 and a plate scale of 7.39mm/nm from the optical design yields $\Delta\lambda = F$ = 51 μm (~3.4 pixels). The fiber input D = 1.2″ projects to 120 μm at the telescope focal plane. Assuming octagonal fibers paired with a ball lens double scrambler[11] SG is about 13,000, so being conservative for the RV budget we assume a value of SG=8,000 for added margin.

We translate the desired RV error limit δv=0.1m/s to wavelength shifts using the Doppler-equation: $\delta\lambda = (\delta v / c) \cdot \lambda$. By associating this $\delta\lambda$ wavelength shift on the detector with f, and using the a plate scale of 7.39mm/nm, we can transform the allocation of velocity error in the RV budget to a Tracking Error requirement of the telescope and tip-tilt system by re-arranging the definition of the scrambling gain: $d = D \cdot SG \cdot (f/F)$ = 0.4″. We do expect the telescope tracking to perform much better than this. Our allocations for guiding accuracy, however, is set much stricter than above derived 0.4″, for multiple reasons:

- in order to have the ability to potentially reach the 0.1m/s RV error goal of the EPDS program it is advised to keep error sources below that limit by a factor of a few, thus shooting for (0.4″/3)≈0.1″ tracking;
- better tracking accuracy improves throughput;
- the WIYN telescope is already operating at the limit of the drive system, and adding on the Front End to a completely undeveloped port could bring up unforeseen guiding issues;
- by implementing a precise tip-tilt/guding system, which is relatively straightforward, provides a general reserve in case the fiber system and scrambler does not meet predicted performance.

Other bottom-level branches in this trunk – ADC Performance, Telescope Focus, and Flexure/Thermal Variation Post-Calibration – affect the illumination of fiber inputs, which in turn change the intensity distribution at the fiber output. Such near-field effects which move the line centroids (i.e. pointing and tracking) are most significant, but far field effects which affect higher order moments of the PSF stability (i.e. line shapes, width, skewness, kurtosis) are also present. We have used the EchMod software package[17] to simulate RV errors arising from extreme cases of non-uniform illumination of the spectrograph pupil (i.e. far-field instabilities), for details see [12].

These sources constitute the bottom level of the non-calibratable instrument error branch of the RV error budget, indicated in orange as allocations in Figure 15. These terms are RSS summed (blue symbols) with the barycentric error (indicated in green for analysis) to derive the total 0.34m/s error that drives the overall budget. Similar procedures are used to justify our estimates of the post-calibration residual trunk.

4.SELECT DESIGN ELEMENTS AND LESSONS LEARNED

Pupil slicing

PRV spectrographs designed for extremely large telescopes[18] (ELTs) understandably can benefit from pupil slicing, as Eq. 1 clearly shows. If not the budget then the limited size/availability of gratings and refractive substrates for the camera optics could be prohibitive to even build them. Image slicing or the use of adaptive optics[19] can also shrink the size of PRV instruments. For WISDOM, which is designed for a 3.5m telescope like the one HARPS uses, does not necessarily require pupil slicing as conventional optical designs, like HARPS, are clearly feasible. However, as we showed, the relatively small added complexity of the fiber feed or fiber run can result in significant budget savings – which we decided to recycle into the instrument by expanding its wavelength coverage and also to break up that wide passband into multiple cameras. This, in turn, resulted in the excellent efficiency of WISDOM. Besides that clear advantage the small instrument size allowed us to design around commercial off the shelf (COTS) components, shortening the delivery schedule and minimizing associated risks, which was very important to meet the highly aggressive delivery schedule dictated by the EPDS program requirements.

The pupil slicing also can be done microscopically, using a fiber based slicer, either at the fiber feed at the telescope or further downstream in the fiber link or just before the spectrograph slit. Such solution would impose a different set of design problems than ours, but both are feasible – in fact we did demonstrate our solution by building a prototype during the instrument concept study phase, and MAROON-X is working on a fiber-based prototype[20].

Thus we strongly suggest that the application of slicing, or use of adaptive optics, is a technique that PRV instruments should look into very closely, even if the telescope size would not demand the use of these advanced techniques.

Optical design choices

The WISDOM optical design[12] cleverly utilizes a symmetrical and balanced arrangement of optical elements, which results in a very simple optical bench. In some ways the ability to do so was also the result of pupil slicing and the re-investment of the achieved budget savings into multiplication of the spectrograph and cameras. The 4 cameras were also designed with a constraint to follow the same (or at least very similar) optical formula, so that the opto-mechanical design elements could be recycled and thus allow savings by non-reoccurring engineering costs. The WISDOM camera designs[12] do not follow the recent trend[21,22] of employing very few elements (4-5) that exploit the fact that echelle spectrograph cameras do not have to be corrected either for lateral or axial color (chromatic focal shift). Latter now is often compensated by the tilt of the detector. The argument is clear: simple cameras, few elements to decrease cost and for increased throughput, and in some cases the avoidance of ghosts. (In fact it might be an effective, alternative solution to combat VPH recombination ghosts without slanting the VPH fringes.) However, these cameras cannot be fully tested independently, only within the optical framework of the spectrograph, or just partially using (quasi-)monochromatic beams and/or scanning the field. We yet to see how this will work out, as the first such instruments go through the AI&T and commissioning.

We argue that for PRV instruments these simplified camera designs might be not the optimal approach, where minuscule variations of the PSF, static (as frozen in by the design, manufacturing errors and alignment) and/or dynamic (latter due to pupil illumination variations), can have severe effects on the ability to deduce sub-m/s RV values. It is probably more advantageous to have the added degrees of design freedom, granted by the larger number of optical elements, to carefully sculpt the PSF and make it robust in a sense that its variation as a function of wavelength and its sensitivity against changes of pupil illuminations is minimized. It is also more convenient and reassuring if the cameras can be fully and independently tested before inserting them into the spectrograph. Especially for vacuum enclosed or cryogenic instruments, for which AI&T schedule can be significantly impacted by the added complexity of aligning these simpler few element cameras.

For WISDOM we did not have to worry about throughput hit or increased cost due to the larger number of camera lens elements, as the passband of each camera was very narrow allowing for efficient AR coatings and optimal glass selection. Also the asymmetric white pupil design and pupil slicing resulted in a very modest pupil size and thus small, cheap lenses. The lack of aspheres in the camera design was a conscious design choice as well, since manufacturing and alignment errors of such optical elements can have a more significant effect on the behavior of the PSF, something we had been very concerned about as mentioned above.

Last but not least we would like to point out the use of a Mangin mirror that also simplifies camera design and benefits the behavior of the PSF. After the re-introduction of this idea by the G-CLEF instrument[18] some recent PRV spectrographs[23] also employ this solution, and in our opinion it should be considered by other recent/future designs due to its significant benefits.

A warm NIR channel

The NIR arm of WISDOM in particular facilitates studies of low-mass stars that are most likely to host *TESS*' habitable zone planets, as well as the identification and suppression of astrophysical noise or stellar jitter. It also addresses the second recommendation of the ExoPAG study group[1] at much lower cost than a separate

instrument, and so we were keen on its implementation, following the philosophy of WINERED[24] that employs a 1.7μm cut-off HgCdTe sensor along with a thermal blocking filter. We planned to implement this filter via interference coatings on the camera lenses, and have been actively working with Infinite Optics on such design. However, there are a couple things that is worth mentioning and discussing in this context. The first is about the true sensitivity of the mentioned detectors beyond their 1.7μm cut-off. Some recent investigations[25] indicate the the so-called Urbach-tail[26] might not level out at practically zero sensitivity beyond the cut-off. Also, while the coating designs predicted superb performance, and similar coatings were delivered by the vendor previously on silicon substrates, our first attempts of implementing those complex (80+ layers) interference filters on glass failed due to partial delamination. While we achieved good progress with alternative designs, leveraging on substrate-based absorption in combination with a somewhat simpler layer structure, it still remains an open issue. We would like to point out, though, that a very important aspect of such design that was overlooked in some earlier similar attempts, is the filter performance over a wide range of angle of incidences (AOIs). While a spectrograph camera has a relatively small field angle (~10-20°), the thermal radiation from a non-cryogenic instrument sends NIR rays towards the detector at much higher AOIs, and thus the filter needs to efficiently eliminate those as well. Alternatively, or in combination with that, a cold baffle can be sufficient, although implementation of such within an otherwise non-cryogenic instrument can impose some challenges.

Use of carbon fiber, and the choice of small vs. "brand name" vendors

CFRP seems to appear in more and more ground based instruments, from (vacuum enclosed) optical benches[27] to vacuum vessels[28]. While this is an engineered material, and such its properties vary depending on manufacturing technique and vendors, it seems to be a mature and well-understood technology by now with plenty of companies on the market. Like invar, that is also an engineered material but by now well accepted and widely used in instrumentation, CFRP might be a bit overlooked despite being a viable and readily available design choice, even for vacuum related applications. Our experience with the WISDOM Front End design showed that there could be an order of magnitude difference in price for a given component – despite that the structural analysis and manufacturing study made by the companies themselves indicated very comparable performance. Our choice thus turned out to be not a large brand name company but rather the relatively small CarbonVision GmbH in Germany. They might no offer plenty of space flight heritage, but do some, and more importantly have impressive references such as the LINC-NIRVANA optical bench, multiple telescope port adaptors, etc. For such smaller companies the agility, direct access to engineering knowledge can be very satisfying and make the design and implementation very efficient. Although on the other hand one always has to be careful to fully understand the momentarily dynamics and readily available resources that can quickly change for smaller firms, and can severely affect delivery schedule.

Fiber customization and testing, and the importance of early prototyping

To maximize throughput of the fiber link, by minimizing focal ratio degradation (FRD) losses, we engaged with a vendor to custom draw octagonal core fibers[7] with non-conventional numerical aperture. While this seemed to be relatively straight-forward process based on strong heritage, it turned out to be much more complicated and much more expensive than we or the vendor thought. Since it was a customization we opted for early prototyping, and as it turned out we were very glad we did so. The lesson learned there is that sometimes vendors themselves can be mistaken and overly confident about something that is just a bit different than what they do on a regular basis. This is a small, but we think a valuable cautionary tale to be considered when making risk assessment of a design concept. Another part of the lesson is the "trust but verify" approach, since the vendor might not be able to fully characterize and assess the small requested deviation from the norm. So it is either on the designer, or as in our case the willing vendor, to implement new, improved test and evaluation methods and/or hardware.

Effect of Optical Design on sub-m/s Radial Velocities

For PRV instruments this is a very fundamental issue, and while recently has been discussed in some papers[18,21,22,23] there is yet a fully dedicated study to be written on the topic. While this present paper did not discuss the optics in detail, we refer to the accompanying WISDOM optical design paper[12], as we feel the issue is important enough to be listed here in this section.

Our realistic simulations of the as-built cameras, and generation then subsequent reduction of simulated 2D echellogram spectra, led to an important discovery: the unexpectedly high vulnerability of RV stability to fluctuations in the far-field illumination (<~1% changes in intensity distributed across the pupil). We developed a new method for analyzing this problem in the context of the realistically achievable optical alignment and tolerance stack-up. Through the process we discovered a source of RV errors at the m s^{-1} level that not only needs to be considered for WISDOM, but may also be relevant to other currently operating PRV instruments, even if those were designed consciously not to be sensitive to pupil illumination changes. We plan to describe these findings and the analysis in a subsequent paper.

The Value of a Solar Telescope

A very cheap and simple solar telescope provides an ability to study the performance of the spectrograph during day-time, and we think it is an invaluable tool to speed up on-site commissioning and to continuously monitor instrument health/performance, even in periods when the spectrograph is not scheduled at night. Additionally, prototype spectra can be already acquired in the AI&T laboratory, to be used for early tests and to begin tuning the data reduction pipeline on real stellar exposures long before on-site commissioning.

5.SUMMARY

One of the two NASA-NSF funded extreme precision Doppler spectrograph instrument concept studies is led by the Massachusetts Institute of Technology, in consortium with Lincoln Laboratories, Harvard-Smithsonian Center for Astrophysics and the Carnegie Observatories. This paper described the instrument concept WISDOM (WIYN Spectrograph for DOppler Monitoring) prepared by this team.

WISDOM is a four-channel fiber-fed échelle spectrograph with continuous wavelength coverage from 380-1300nm. The resolution is 110,000 in the default High Throughput mode, and 160,000 in the ancillary High Resolution mode. Such high resolution —critical for PRV science— ordinarily requires a large and costly instrument. WISDOM uses a novel pupil slicer to achieve high resolution with a compact and cost-effective design. The pupil slicer splits the telescope's effective aperture into six symmetric segments, each of which feeds a dedicated optical fiber. The fibers send light into the environmentally-controlled spectrograph, where the light is divided by dichroic mirrors into four channels: Blue (380-480nm), Green (480-750nm), Red (750-950nm), and Near-Infrared (950-1300nm). Each channel has its own camera, with wavelength-optimized coatings and detectors. This design allows four PRV spectrographs to fit into a single vacuum enclosure that is readily accommodated within the available space at the WIYN observatory.

WISDOM achieves a radial-velocity precision of at least 0.5m/s through subsystems that mitigate the variations imparted by the telescope and atmosphere, and deliver the light to an ultra-stable spectrometer. These subsystems (i) remove atmospheric dispersion and telescope tracking errors, stabilizing the stellar image on the input optical fibers, (ii) doubly scramble the near- and far-field illumination patterns, producing a uniform intensity distribution from the output fiber, and (iii) maintain a thermally stable ($\Delta T \sim 1mK/24hrs$) vacuum environment for the optical system. The optical system is designed to minimize image motion shifts from thermal-mechanical drifts on long timescales, and changes in input illumination, either of which would otherwise lead to spurious Doppler signals and mask the signals of low-mass planets.

Precise calibration of the wavelength scale is achieved with a GPS-referenced Laser Frequency Comb, which sends calibration light directly into the spectrometer for contemporaneous integration with stellar spectra. Calibration light can also be fed through the pupil slicer and science fibers, to characterize any apparent wavelength shifts arising from these elements. Data reduction is achieved with a software pipeline based on an existing, highly successful code that has been used most recently for HARPS-N. Starting from raw image frames, the pipeline produces 1D wavelength-calibrated spectra and RV measurements, which are sent to the EPDS data archive. The pipeline also uses (and archives) telemetry from the instrument, for recognition and removal of systematic effects.

The other EPDS proposal that finally got selected in March 2016 by NASA, after the ICS phase and the submission of this paper, was prepared by a consortium under the lead of Principal Investigator Suvrath Mahadvean at the Penn State University. Their instrument, called NEID (NN-EXPLORE Exoplanet Investigations with Doppler Spectroscopy), builds on the heritage of the nearly completed Habitable Planet Finder instrument[29], which is designed and built largely by the same team and soon to be commissioned on the HET. For more details about those project see the Penn State blogs (hpf.psu.edu, neid.psu.edu) and related papers[22,29,30,31].

REFERENCES

[1] P. Plavchan, D. Latham, S. Gaudi, J. Crepp, X. Dumusque, G. Furesz, A. Vanderburg, C. Blake, D. Fischer, L. Prato, R White, V. Makarov, G. Marcy, K. Stapelfeldt, R. Haywood, A. Collier-Cameron, A. Quirrenbach, S. Mahadevan, G. Anglada, P. Muirhead, "Radial Velocity Prospects Current and Future: A White Paper Report prepared by the Study Analysis Group 8 for the Exoplanet Program Analysis Group (ExoPAG)", arXiv: 1503.01770 (2015)

[2] F. Fressin, G. Torres, D. Charbonneau, S. T. Bryson, J. Christiansen, C. D. Dressing, J. M. Jenkins, L. M. Walkowicz, and N. M. Batalha, "The false positive rate of Kepler and the occurrence of planets", ApJ, 766, 81 (2013)

[3] D. Spergel, N. Gehrels, C. Baltay, D. Bennett, J. Breckinridge, M. Donahue, A. Dressler, B. S. Gaudi, T. Greene, O. Guyon, C. Hirata, J. Kalirai, N. J. Kasdin, B. Macintosh, W. Moos, S. Perlmutter, M. Postman, B. Rauscher, J. Rhodes, Y. Wang, D. Weinberg, D. Benford, M. Hudson, W. -S. Jeong, Y. Mellier, W. Traub, T. Yamada, P. Capak, J. Colbert, D. Masters, M. Penny, D. Savransky, D. Stern, N. Zimmerman, R. Barry, L. Bartusek, K. Carpenter, E. Cheng, D. Content, F. Dekens, R. Demers, K. Grady, C. Jackson, G. Kuan, J. Kruk, M. Melton, B. Nemati, B. Parvin, I. Poberezhskiy, C. Peddie, J. Ruffa, J. K. Wallace, A. Whipple, E. Wollack, F. Zhao, "Wide-Field InfrarRed Survey Telescope-Astrophysics Focused Telescope Assets WFIRST-AFTA 2015 Report", arXiv:1503.03757 (2015)

[4] P. W. Sullivan, J. N. Winn, Z. K. Berta-Thompson, D. Charbonneau, D. Deming, C. D. Dressing, D. W. Latham, A. M. Levine, P. R. McCullough, T. Morton, G. R. Ricker, R. Vanderspek, D. F. Woods , "The Transiting Exoplanet Survey Satellite: simulations of planet detections and astrophysical false positives", ApJ 809, 77 (2014)

[5] Bouchy, F., Pepe, F., Queloz, D., "Fundamental photon noise limit to radial velocity measurements", Astronomy and Astrophysics v.374, p.733-739 (2001).

[6] J. M. Irwin, Z. K. Berta-Thompson, D. Charbonneau, J. Dittmann, E. E. Falco, E. R. Newton, P. Nutzman, "The MEarth-North and MEarth-South Transit Surveys: Searching for Habitable Super-Earth Exoplanets Around Nearby M-dwarfs", arXiv:1409.0891 (2011)

[7] Fűrész, G., R. Pawluczyk, P. Fournier, R. Simcoe, D. F. Woods, "Fiber link design for the NASA-NSF extreme precision Doppler spectrograph concept WISDOM", Proc. SPIE 9908, 9908-281, these proceedings (2016).

[8] Neuschaefer, L.W. & Windhorst, R.A., "Observation and reduction methods of deep palomar 200 inch 4-shooter mosaics", AJ Suppl., 96, 371-399 (1995)

[9] Robin, A. C.; Reylé, C.; Derrière, S.; Picaud, S, "A synthetic view on structure and evolution of the Milky Way ", A&A., 409, 523 (2003)

[10] M. Egan, G. Furesz, R. Foster, R. Simcoe, "Pupil slicer design for the NASA-NSF Extreme Precision Doppler Spectrograph concept WISDOM", Proc. SPIE 9912, 9912-183, these proceedings (2016)

[11] S. Halverson, A. Roy, S. Mahadevan, L. Ramsey, E. Levi, C. Schwab, F. Hearty, N. MacDonald, "An efficient, compact, and versatile fiber double scrambler for high precision radial velocity instruments", ApJ 806, 61 (2015)

[12] S. Barnes, G. Furesz, R. Simcoe, S. Shectman, D. F. Woods, "Optical design of the NASA-NSF Extreme Precision Doppler Spectrograph concept WISDOM", Proc. SPIE 9908, 9908-247, these proceedings (2016)

[13] X. Dumusque, A. Glenday, D. F. Phillips, N. Buchschacher, A. Collier Cameron, M. Cecconi, D. Charbonneau, R. Cosentino, A. Ghedina, D. W. Latham, C-H. Li, M. Lodi, C. Lovis, E. Molinari, F. Pepe, S. Udry, Di. Sasselov, A. Szentgyorgyi, R. Walsworth, "HARPS-N observes the Sun as a star", ApJL 814, L21 (2015)

[14] HARPS user manual, 3P6-MAN-ESO-90100-0005, Issue 2.1, October 1, 2011, www.eso.org

[15] Podgorski, W.; Bean, J.; Bergner, H.; Chun, M-Y.; Crane, J.; Evans, I.; Evans, J.; Furesz, G.; Guzman, D.; Kim, K-M.; McCracken, K.; Mueller, M.; Norton, T.; Park, C.; Park, S.; Plummer, D.; Szentgyorgyi, A.; Uomoto, A.; Yuk, I-S., "A novel systems engineering approach to the design of a precision radial velocity spectrograph: the GMT-Consortium Large Earth Finder (G-CLEF)", Proc. SPIE 9147, 9147-8WP (2014)

[16] Avila, G. and Singh, P., "Optical fiber scrambling and light pipes for high accuracy radial velocities measurements", Proc. SPIE 7018, 70184W (2008)

[17] Barnes, S., "EchMod: a MATLAB toolbox for modeling astronomical échelle spectrographs", Proc. SPIE 8550, 85501T (2012)

[18] Furesz, G., Epps, H., Barnes, S., Podgorski, W., Szentgyorgyi, A., Mueller, M., Baldwin, D., Bean, J., Bergner, H., Chun, M-Y., Crane, J.; Evans, J., Evans, I., Foster, J., Gauron, T., Guzman, D., Hertz, E., Jordan, A., Kim, K-M., McCracken, K., Norton, T., Ordway, M., Park, C., Park, S., Plummer, D., Uomoto, A., Yuk, I-S., "The G-CLEF spectrograph optical design", Proc. SPIE 9147, 91479G (2014)

[19] Crepp, J. R., Bechter, A., Bechter, e., Ketterer, R., "iLocater: An AO-fed Doppler spectrometer for the Large Binocular Telescope", Proc. SPIE 9908, 9908-46, these proceedings (2016)

[20] Seifahrt, A., Stürmer, J., Bean J. L., "A micro-lens array based pupil slicer and double scrambler for MAROON-X", Proc. SPIE 9908, 9912-61, these proceedings (2016)

[21] P. Spano, B. Delabre, H. Dekker, F. Pepe, F.M. Zerbia, P. Di. Marcantonio, S. Cristiani, D. Megevand, "Very high-resolution spectroscopy: the ESPRESSO optical design", Proc. SPIE 8446, 84467V (2012)

[22] C. Schwab, A. P. Rakich, S. Mahadevan, S. P. Halverson, Q. Gong, J. Stürmer, Y. V. Gurevich, E. I. Levi, F. R. Hearty, R. C. Terrien, P. M. Robertson, A. J. Monson, J. T. Wright, M. W. McElwain, C. F. Bender, C. H. Blake, A. G. Chakraborty, L. W. Ramsey, "Optical design for NEID, a proposed spectrometer for NASA's WIYN extreme precision Doppler spectrometer", Proc. SPIE 9908, 9908-282, these proceedings (2016)

[23] C. A. Jurgenson, D. A. Fischer, T. M. McCracken, D. G. Sawyer, A. E. Szymkowiak, G. P. Muller, F. G. Santoro, "EXPRES: a next generation RV spectrograph in the search for earth-like worlds", Proc. SPIE 9908, 9908-258, these proceedings (2016)

[24] S. Kondo, Y. Ikeda, N. Kobayashi, C. Yasui, H. Mito, K. Fukue, K. Nakanishi, T. Kawanishi, T. Nakaoka, S. Otsubo, M. Kinoshita, A. Kitano, S. Hamano, M. Mizumoto, R. Yamamoto, N. Izumi, N. Matsunaga, H. Kawakita, "A Warm Near-Infrared High-Resolution Spectrograph with Very High Throughput (WINERED)", arXiv: 1501.03403 (2015)

[25] R. C. Terrien, S. Mahadevan, L. W. Ramsey, S. P. Halverson, C. F. Bender, A. Monson, "A thermal blocking filter reveals the extended red sensitivity of a 1.7 micron cutoff H2RG detector", Proc. SPIE 9915, 9915-62, these proceedings (2016)

[26] Urbach, F., "The Long-Wavelength Edge of Photographic Sensitivity and of the Electronic Absorption of Solids", Phys. Rev. 92, 1324 (1953)

[27] D. Baldwin, W. A. Podgorski, M. A. Mueller, K. McCracken, H. Bergner, J. Foster, "Advanced structural design for precision radial velocity instruments", Proc. SPIE 9912, 9912-121, these proceedings (2016)

[28] C. Padilla, L. Cardiel-Sas, O. Ballester, F. Graña̋ena, L. Lopez, E. Majà, F. J. Castander, "The PAU Camera carbon fiber cryostat and filter interchange system", Proc. SPIE 9908, 9908-167, these proceedings (2016)

[29] S. Mahadevan, T. B. Anderson, C. F. Bender, S. P. Halverson, F. R. Hearty, E. I. Levi, Y. Li, A. J. Monson, M. J. Nelson, L. W. Ramsey, P. M. Robertson, A. Roy, C. Schwab, G. K. Stefánsson, R. C. Terrien, "The Habitable-zone Planet Finder: AI&V status and summary of research and development to achieve high precision NIR Doppler radial velocities", Proc. SPIE 9908, 9908-40, these proceedings (2016)

[30] S. P. Halverson, R. C. Terrien, S. Mahadevan, C. F. Bender, A. Roy, G. K. Stefansson, A. J. Monson, E. I. Levi, F. R. Hearty, C. H. Blake, M. W. McElwain, C. Schwab, L. W. Ramsey, S. X. Wang, J. T. Wright, Q. Gong, "A comprehensive radial velocity error budget for next generation Doppler spectrometers", Proc. SPIE 9908, 9908-254, these proceedings (2016)

[31] P. M. Robertson, F. R. Hearty, T. B. Anderson, G. K. Stefánsson, E. I. Levi, C. F. Bender, S. Mahadevan, S. P. Halverson, A., J. Monson, L. W. Ramsey, A. Roy, C. Schwab, R. C. Terrien, M. J. Nelson, B. Blank, "A system to provide sub-milliKelvin temperature control at T~300K for extreme precision optical radial velocimetry", Proc. SPIE 9908, 9908-228, these proceedings (2016)